### Title
In vivo multiphoton fluorescence imaging: A novel approach to oral malignancy




### Journal
Lasers in Surgery and Medicine, 35(2)

### ISSN
0196-8092



### Authors
Wilder-Smith, Petra
Osann, Kathryn
Hanna, Nevine
et al.



### Publication Date
2004-08-01

### DOI
10.1002/lsm.20079

# In Vivo Multiphoton Fluorescence Imaging: A Novel Approach to Oral Malignancy

**Petra Wilder-Smith, DDS, PhD,[1]* Kathryn Osann, PhD,[2] Nevine Hanna, BS,[1] Naglaa El Abbadi, BS,[1] Matt Brenner, MD,[2] Diana Messadi, DDS, DMSc,[3] and Tatiana Krasieva, PhD[1]**

[1]*Beckman Laser Institute, University of California, Irvine California 92612*

[2]*University of California, Irvine California 92612*

[3]*University of California, Los Angeles, California 90095*

**Background and Objective:** Current techniques for oral diagnosis require surgical biopsy of lesions, and may fail to detect early malignant change. Non-invasive, sensitive tools providing early detection of oral cancer and a better understanding of malignant change are needed. These studies evaluated in vivo multiphoton excited fluorescence (MPM) techniques to (1) map epithelial and subepithelial changes through out oral carcinogenesis and (2) serve as an effective diagnostic modality.

**Study Design/Materials and Methods:** In the hamster model (n = 70), epithelial and subepithelial change was imaged in vivo throughout carcinogenesis. MPM- and histopathology-based diagnoses on a scale of 0 (healthy)–6 (squamous cell carcinoma [s.c.c.]) were scored by two pre-standardized investigators.

**Results:** Collagen matrix and fibers, cellular infiltrates, blood vessels, and microtumors were clearly visible. MPM agreed with the histopathology for 88.6% of diagnoses.

**Conclusions:** In vivo MPM images provide (1) high resolution information on specific components of the carcinogenesis process (2) an excellent basis for oral diagnostics. Lasers Surg. Med. 35:96–103, 2004.



**Key words:** carcinoma; non-invasive imaging; leukoplakia; non-invasive diagnostics; oral diagnosis

## INTRODUCTION

Despite significant advances in cancer treatment, early detection of cancer and its curable precursors remains the best way to ensure patient survival and quality of life. Oral cancer will claim approximately 10,000 lives in the US this year [1–3]. Accounting for 96% of all oral cancers, squamous cell carcinoma (s.c.c.) is usually preceded by dysplasia presenting as white epithelial lesions on the oral mucosa (leukoplakia). Leukoplakias develop in 1–4% of the population [2]. Malignant transformation, which is quite unpredictable, occurs in 1–40% of leukoplakias over 5 years. Dysplastic lesions in the form of erythroplakias carry a risk for malignant conversion of approximately 90% [2]. Tumor detection is complicated by a tendency towards field cancerization, leading to multicentric lesions [4]. Current techniques require surgical biopsy of lesions, which are often benign, yet they detect malignant change too late for optimal treatment response in many cases. Of all oral cancer cases documented by the National Cancer Institute Surveillance, Epidemiology and End Results Program, advanced lesions outnumbered localized lesions more than 2:1. Five-year survival rate is 75% for those with localized disease at time of diagnosis, but only 16% for those with cancer metastasis [2,3]. A modality for direct, non-invasive early detection, diagnosis and monitoring of oral dysplasia and malignancy and screening of high-risk populations is urgently required to identify treatment needs at an earlier, more treatable stage of pathological development. Such a multi-use clinical capability would immediately produce a sharp drop in morbidity and mortality due to cancer, with enormous reductions in patient anxiety and suffering as well as treatment cost.

A better understanding of the processes related to malignant change is also needed to improve and monitor the effectiveness of interventions available to patients. Precancers are characterized by epithelial changes including increased nuclear size, increase nuclear-to-cytoplasmic ratio, hyperchromasia, pleomorphism, angiogenesis, and increased metabolic rate [5]. Epithelial invasion of underlying structures marks the transition to full-blown malignancy. The neoplastic process is associated with changes in the extracellular matrix (ECM), especially the collagen fibers and the framework that they constitute. Several authors have described collagen loss in malignancy, although the time- and spatially-resolved sequence of this

Contract grant sponsor: CPRF; Contract grant numbers: 27722, 30003. Contract grant sponsor: CCRP; Contract grant number: 00-01391V-20235; Contract grant sponsor: NIH; Contract grant numbers: R021 CA8752701, EB-00293 CA91717; Contract grant sponsor: TRDRP; Contract grant number: 71T-0192; Contract grant sponsor: NIH (LAMMP); Contract grant number: RR01192; Contract grant sponsor: DOE; Contract grant number: DE903-91ER 61227; Contract grant sponsor: NSF; Contract grant number: BES-86924; Contract grant sponsor: PMUSA; Contract grant number: 32598; Contract grant sponsor: University of California; Contract grant sponsor: Irvine Chao Family Comprehensive Cancer Center.

*Correspondence to: Petra Wilder-Smith, DDS, PhD, Beckman Laser Institute, 1002 Health Sciences Road East, University of California, Irvine CA 92612. E-mail: pwsmith@bli.uci.edu

Accepted 25 April 2004
Published online in Wiley InterScience (www.interscience.wiley.com).
DOI 10.1002/lsm.20079

process remains undefined [5–9]. Angiogenesis and altered tissue perfusion and oxygenation are also implicated in neoplasia, but again, the specific sequential, spatial, and functional relationship between vascularization and neoplasia has not been clearly elucidated [5,6].

To date, the inability to perform sequential atraumatic in vivo investigations has been a major obstacle to a better understanding of the carcinogenesis process, and to the evaluation and development of novel diagnostic modalities. In this study, we used novel in vivo non-invasive multi photon excited fluorescence (MPM) imaging techniques to image and quantify neoplasia-related epithelial and subepithelial changes at specific locations and stages throughout carcinogenesis in the hamster cheek pouch model.

### MPM and Second Harmonic Generation (SHG) Imaging

MPM is a nonlinear high resolution optical method used in a variety of biological imaging applications [10,11]. The image-forming signal in MPM arises from the simultaneous interaction of two or more photons with the sample. Two-photon interactions in MPM result in SHG and two-photon excited fluorescence (TPF) [12–15]. In TPF, two near-infrared (NIR) wavelength photons are simultaneously absorbed, resulting in the emission of a longer wavelength photon [16]. TPF may be observed depending on energy dissipation pathways of chromophores present in the examined specimens. Fluorescence spectra from two-photon absorption will not necessarily resemble spectra from linear spectroscopy. In SHG, the two NIR wavelength photons interact within the specimen to form a single photon of half the wavelength of the incident field.

Endogenous SHG in biological materials arises from the large molecular anisotropy and second-order nonlinear susceptibility typical of biological molecules and structures [17]. Collagen appears to be the tissue constituent mainly responsible for SHG [18,19]. Collagen molecules consist of three peptide chains that form a rod-shaped triple helix. Nonlinear susceptibility is an optical property characteristic of chiral molecules. The microcrystalline structure of collagen [21–24] makes it capable of SHG [19,20]. Several researchers have reported endogenous second harmonic generation in biological tissues. Fine and Hansen [18] used a ruby laser to irradiate a variety of excised tissues. SHG was observed only in collagenous tissues (cornea, sclera, tendon, and skin). Cross-beam scanning SHG microscopy was studied in transmission geometry to show detailed variation of collagenous filaments in rat tail tendon [19]. The dependence of the SHG signal on tissue structure and local symmetry has been used for macroscopic mapping [20,21]. SHG was observed in type I collagen by nanosecond laser irradiation over a broad spectral region [21].

MPM permits surface and subsurface high-resolution imaging and measurement of specific tissue components such as collagen, elastin, NADH, and flavins. Many wavelengths can be used; visualization/analysis of deeper subsurface structures such as components of the extracellular matrix, cellular and vascular elements is possible [22–28].

Goal of these preliminary studies were to determine whether premalignant and malignant transformation can be detected and analyzed in vivo using the proposed non-invasive approaches. Specifically, our aims were to identify during carcinogenesis in the hamster cheek pouch model (1) to what extent MPM can detect changes in tissue collagen and ECM, cellular and vascular presence and (2) compare these data with histopathological diagnosis and staging.

## MATERIALS AND METHODS

### Animal Model

The standard Golden Syrian Hamster (*Mesocricetus auratus*) cheek pouch model was used. By application of 0.5% DMBA (9,10 dimethyl-1,2-benzanthracene (Sigma, St. Louis, MO) in mineral oil three times per week, mild to severe dysplasia developed at 3–6 weeks, progressing to s.c.c. at 8–12 weeks. Histological features in this model have been shown to correspond closely with premalignancy and malignancy in human oral mucosa [29]. The median lining wall of one cheek pouch of each hamster was treated with carcinogen. Mineral oil only was applied using the same technique to the control cheek pouch of each animal. The study used 70 female animals, 10–12 weeks old. One animal died at 2 days carcinogenesis, leaving a total of 69 animals in this study. To improve study logistics, the animals were randomly divided into 7 groups of 10 animals each. Only when all the animals from one group had been imaged and sacrificed was the next group incorporated into the study. The animals were housed and treated in accordance with animal research committee guidelines at the University of California, Irvine (approval 97-1972). Previous studies have shown that this carcinogenesis process in one cheek pouch does not affect the other cheek pouch [30,31], and that therefore the untreated cheek pouch can be used as control.

### Protocol

During carcinogenesis over a 15 week period, in vivo (i) clinical evaluation and photography, (ii) MPM were performed at weekly intervals. During in vivo measurements, the cheek pouch was continuously irrigated with isotonic saline at room temperature to avoid dehydration. The animals were kept warm using a heating pad and a thermal sock. Use of these measures eliminated animal mortality almost completely during the sometimes lengthy imaging sessions: only one unplanned animal death occurred throughout the duration of these investigations. Early imaging sessions could last up to 30 minutes; once our techniques were established imaging sessions averaged $<$10 minutes. The anesthetized hamster's everted cheek pouch was attached to the microscope stage using a specially designed and fabricated ring-shaped clamp rigidly fastened to the stage surface (Fig. 1). The clamping device was marked on its rim at 1 mm intervals to allow the use of localization coordinates for designating areas of specific interest and for achieving repeated, atraumatic scans with different modalities in exactly the same location.

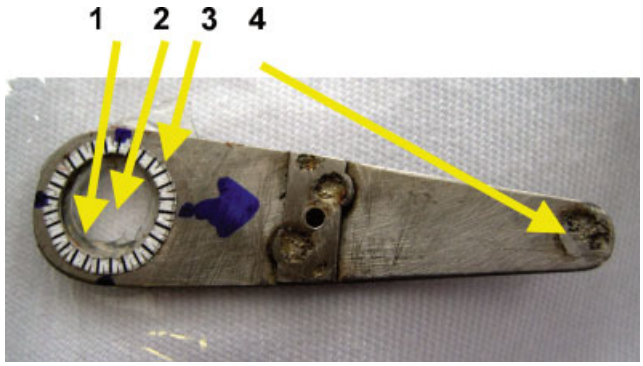


Fig. 1. Hamster cheek pouches held with external fixation device for in vivo multi photon excited fluorescence (MPM). 1: Soft rubberized internal surface of clamp. 2: Window for MPM imaging. 3: Millimeter coordinates for localization of measurements. 4: Area clamped to microscope stage. [Figure can be viewed in color online via www.interscience.wiley.com.]

Accurate re-localization of the clamping device at weekly intervals was ensured by marking several coordinates of the device outline on the hamster cheek pouch using an animal micro tattooing device (Ketchum lab animal micro tattooer, Ottawa, CDN) at least 7 days prior to the commencement of the study. This time frame was selected as preliminary studies had demonstrated the absence of any tattooing-related tissue changes after a minimum of 5 days post-tattooing. While recognizing the value of tattooing in very close proximity to the area of interest to facilitate the co-localization of corresponding MPM images and histopathological sections, this technique was not used to avoid tissue reactive processes to tattooing at a cellular and sub-cellular level. After optical measurements, one animal was sacrificed from each group each week to obtain specimens for routine paraffin embedding and Haematoxylin and Eosin staining. The exception was group 7 (the last group) where one animal was sacrificed weekly beginning with week 6. This was done to permit imaging of cheek pouch changes through the end of week 15; groups 1–6 were imaged through the end of week 11.

### Multi Photon Fluorescence Microscopy

The two-photon laser scanning fluorescence microscope system (Fig. 2) consists of a 5 W Verdi laser (Coherent, Santa Clara, CA) which is used to pump a Titanium:Sapphire (Ti:Al2O3) laser (Mira 900F, Coherent). The mode-locked, 150 femtosecond, 76 MHz pulse train exiting the Ti:Sapphire laser is used as the two-photon pulsed excitation source. The ultrafast Ti:Sapphire laser is configured with a broadband optics set (Coherent) which allows wavelength tunability between 690–1,000 nm. Using the 5 W Verdi pump source, the output power of the Ti:Sapphire laser is ~500 mW. In order to obtain the low average powers required to maintain tissue health at the sample, a half wave plate and polarizer are placed in the input beam path to decrease the average power after the Ti:Sapphire laser and hence the two-photon excitation power. Thus using this ultrafast Ti:Sapphire laser source, low average powers of 5–10 mW can be maintained at the sample while still maintaining sufficient peak power for two-photon excitation to occur. The pulse train exiting the Ti:Sapphire laser is deflected into the back port of a Zeiss Axiovert S100 2TV microscope using a PC controlled galvanometer driven X-Y scanner (Series 603X, Cambridge Technology, Inc., Watertown, MA). Images are generated by raster scanning the x-y mirrors and thus the Ti:Sapphire laser beam across the sample. A custom digital card developed by So et al. at the Laboratory for Fluorescence Dynamics controls the scanner, and a synthesized function generator is used to change

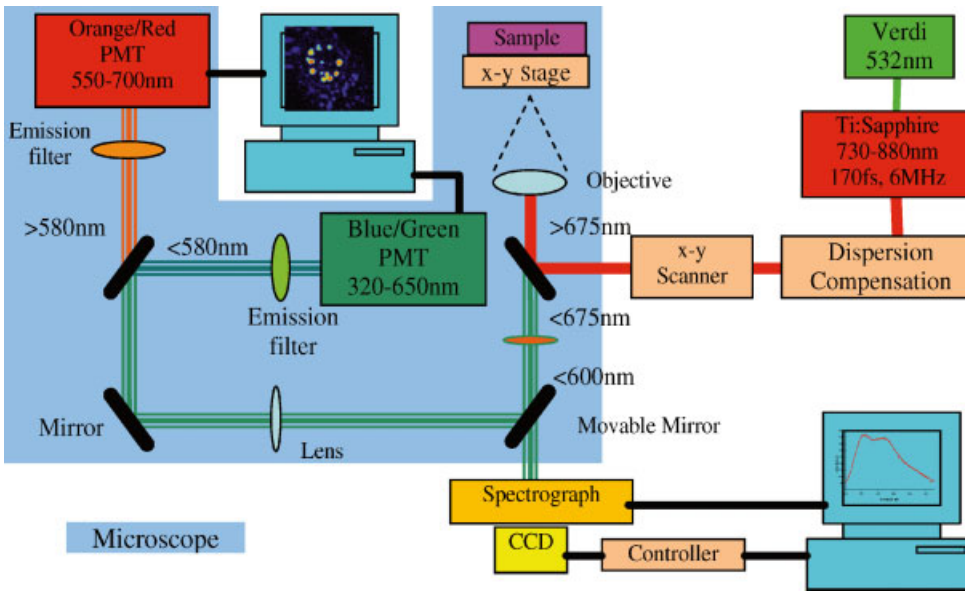


Fig. 2. The MPM System. [Figure can be viewed in color online via www.interscience.wiley.com.]

the scan rate. After passing through the tube lens, the laser excitation light is deflected by a short pass dichroic mirror, and is focused through an objective onto the sample.

Two-dimensional (x-y plane) images (256×256 pixels) are acquired from various depths (z) into the sample at a rate of 1 frame/second (pixel dwell time of 16 μsecond/pixel) with a single-photon counting PMT (R7400P, Hamamatsu Corp., Bridgewater, NJ), covering an area of $35\times35\ \mu m^2$ for the 63× microscope objective. Resolution is approximately 0.4 and 1 μm in the x-y and z image planes, respectively. Each acquired image is typically integrated over 10 seconds. Using this configuration, we routinely obtain tomographic images to depths of 1–1.2 mm within the oral mucosa.

### Histological Evaluation

Histological evaluation of each stained section was quantified by two blinded, pre-standardized scorers (one oral pathologist, one dentist) according to the criteria established by Macdonald [29], whereby each characteristic listed below was assessed. Although a well defined histological grading system for oral epithelial dysplasia has not been developed yet, most oral pathologists grade on the scale of mild-moderate-severe dysplasia depending on the range and severity of individual features and the proportion of epithelium thickness affected. The following numerical grading system was used for each slide: 0, healthy; 1, hyperkeratosis; 2, mild dysplasia; 3, moderate dysplasia; 4, severe dysplasia; 5, carcinoma-in-situ; 6, s.c.c. The criteria for Oral Epithelial Dysplasia were as follows: drop-shaped rete ridges, irregular epithelial stratification, individual cell keratinization, basal cell hyperplasia, loss of intercellular adherence, loss of polarity, hyperchromatic nuclei, increased nucleo-cytoplasmic ratio, anisocytosis, pleomorphic cells and nuclei, abnormal mitotic figures, increased mitotic activity. Each site was assessed for each of these characteristics at a level of either none (0), slight (1), or marked (2).

### MPM Imaging

The areas imaged were selected with the naked eye. All MPM imaging was performed using a 10× objective. In the control cheek pouch, an easily accessible tissue area at the apex of the cheek pouch, circular in shape, 7 mm in diameter, was imaged. Area size was defined by the dimensions of the window in the cheek pouch holder. In the cheek pouch undergoing carcinogenesis, a circular area at the center of the zone of developing pathology was selected using the naked eye. Size was again defined by the 7 mm window in the cheek pouch holder. The entire tissue within the window area was visualized at 10× using the MPM system by slowly scanning across its surface. Five areas (each approximately 1×1 mm) showing the most severe pathological changes were selected for detailed imaging and later diagnostic scoring. The coordinates on the cheek pouch holder of these areas were noted and used for re-imaging the same locations at weekly intervals. The five images from these five areas were grouped as data from one site when presented to the scorers.

### MPM Evaluation

Two blinded, pre-trained investigators classified each image diagnostically on a scale of 0 (normal)–6 (s.c.c.), based on changes in collagen presence, structure, fiber length/organization, cellular exudates, vascularization, and microtumors. Data consisted of descriptive images and included both categorical and continuous variables. For collagen presence, fiber length, matrix structure and organization as well as inflammatory exudates and presence of microtumors, changes were categorized as affecting percentages of image area: none, 1–25%, 25–50%, 51–75%, >75%. Vessel presence and location data were descriptive.

### Scoring Protocol

Scorers were pre-trained using a standard set of 50 MPM and 50 matching histopathological images. Initial training was repeated until at least 90% of images were identified correctly, then 50 new sets of MPM and histopathology images were identified by each scorer with at least 90% accuracy. At this stage, scorers were deemed "pre-standardized" and ready to participate in these studies. Each scorer evaluated all data in one session which took place once all data accrual was complete. A second re-evaluation of all images by the same scorers in one session 3 months later was used to evaluate intra-observer variability.

### Statistical Evaluation

To test for agreement between the two scorers, and between the same scorer at the first and second evaluation of each sample, a kappa statistic was used. A consensus diagnostic score for any specific image was created by taking the average of the two ratings rounded to the nearest whole integer. The histopathology score was used as the gold standard. Because histopathology was classified into seven different categories, agreement between MPM and histopathology was first described by percent agreement, then by sensitivity and specificity which are more appropriate for dichotomous discrete variables. The diagnostic sensitivity and specificity of MPM were defined using two approaches: (1) investigating the ability of MPM to differentiate between healthy (0–1) versus pathological (2–6) lesions, and (2) investigating the ability of MPM to differentiate between malignant (5–6) versus non-malignant (0–4) lesions. These values were calculated considering data from each scorer separately and also using the consensus score.

## RESULTS

The novel in vivo MPM and SHG imaging techniques clearly imaged a wide range of structural and functional characteristics. The presence and structure of the collagen/elastin framework were clearly visible, cellular infiltrates were apparent, normal versus engorged blood vessels could be identified, microtumors were visualized.

Table 1 summarizes the typical features of each histopathological grade or score as visualized using MPM.

**TABLE 1. Percentage Area of MPM Image Typically Affected by Each Level of Pathology**

| Diagnostic score/observation | 0 | 1 | 2 | 3 | 4 | 5 | 6 |
|---|---|---|---|---|---|---|---|
| Collagen presence | 0% | 0% | 1–25% | 26–50% | 51–75% | 51–75% | 51–75% |
| Collagen fiber length | 0% | 1–25% | 1–25% | 26–50% | 51–75% | 51–75% | >75% |
| Collagen matrix organization | 0% | 1–25% | 26–50% | 26–50% | 51–75% | 51–75% | >75% |
| Cellular exudate | 0% | 1–25% | 1–25% | 1–25% | 26–50% | 51–75% | 51–75% |
| Microtumor presence | 0% | 0% | 0% | 0% | 0% | 1–25% | 26–50% |

Imaging area approximated 1 × 1 mm. Diagnostic scoring was on a semiquantitative scale of 0–6: 0, healthy; 1, hyperkeratosis; 2, mild dysplasia; 3, moderate dysplasia; 4, severe dysplasia; 5, carcinoma-in-situ; 6, squamous cell carcinoma.

Collagen fiber length and organization showed changes very early in carcinogenesis (2–3 weeks DMBA), whereas the onset of changes in the collagen presence occurred somewhat later (4–6 weeks). Cellular exudates were common throughout pathogenesis.

In healthy tissue (Fig. 3), a well-structured linear collagen matrix, with long, individual collagen fibers was seen consistently throughout the tissues. Blood vessels as well as cellular components within blood vessels were apparent. In inflamed tissues (Fig. 3), engorged blood vessels were seen within an intact, but looser and less dense collagen matrix. Vessel presence and location appeared normal. Collagen fibrils appeared shorter and the matrix demonstrated less of an interwoven structure. Typically, collagen presence was normal, structure and organization were mildly altered in <25% of image area. Cellular infiltration was seen as diffuse patches of red autofluorescence in <25% of image area.

The interstitial matrix was only partially intact in dysplastic tissues (Fig. 4), with some areas of total collagen loss and other areas with variably reduced matrix structure and density. Typically, collagen presence, fiber length, and matrix structure were all reduced with increasing severity of dysplasia. The collagen matrix presence and structure were altered in 25–75% of image area. Collagen fibers that were present showed marked clumping. Blood vessels were occasionally engorged. Cellular exudates were seen throughout the tissues, typically affecting 25–50% of image area.

Autofluorescence from microtumors was observed in malignant tissues (Fig. 5). In early lesions, these were often very small, localized areas interspersed between remnants of collagen matrix. However, in tissues with advanced tumors, the collagen framework became disrupted to the point of complete disappearance and replacement by microtumors.

Typical results for diagnosis of 35 sites by two pre-trained investigators are depicted in Table 2. Agreement within scorers, between scorers and between modalities was assessed using kappa statistics. Intra-observer agreement for the two modalities (histopathology and MPM) at the two scoring time points ($t_1 = 0$, $t_2 = 3$ months) was excellent. Using the kappa statistic for each of the two observers separately and for the observers combined, intra-observer agreement was greater than 90% for each modality (Table 3).

Overall agreement between readings for MPM and histopathology is shown in Tables 4 and 5. MPM agreed with the histopathology for 62 of 70 (88.6%) readings. (The histopathology was underestimated by one category in three of cases and overestimated in five cases. In no instance was the difference between histopathology and MPM more than one level). Using the kappa statistic, agreement between histopathology and MPM was high: 0.833 (SE = 0.069) for observer 1, 0.900 (SE = 0.055 for observer 2, and 0.867 (SE = 0.044) for the observers combined. Agreement between the two pathologists was high with kappa = 0.800 (SE = 0.074).

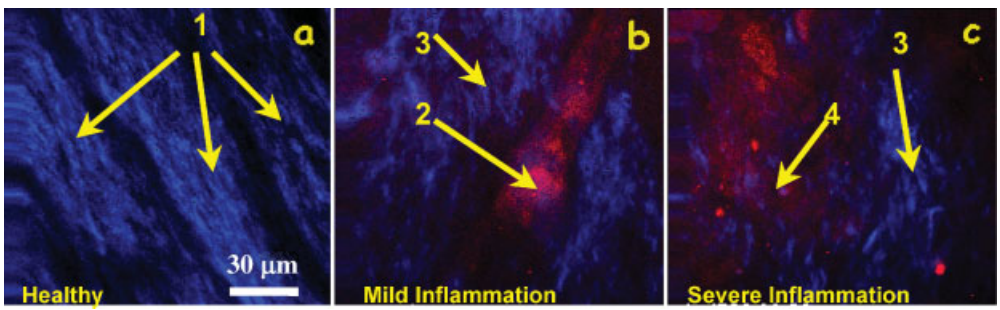


Fig. 3. In-vivo MPM images of normal (**a**) and inflamed (**b**, **c**) hamster check pouch. Second harmonic generation (SHG) largely reflects collagen content of tissue (blue). Note presence of healthy linear collagen matrix (1) throughout the healthy tissues (a). Intact, slightly looser collagen matrix with engorged blood vessel (2) are seen in mild inflammation (b). In inflammation, collagen fibrils appear shorter and fewer (3), matrix less interknit and dense (3) than in healthy tissue (1) (a). More extensively inflamed tissue (c), with cellular infiltration (4). Collagen fibrils are fewer (3). Less linear matrix shows reduced levels of organization (3) than healthy tissues (1)(a). Extensive cellular exudate is present (4).

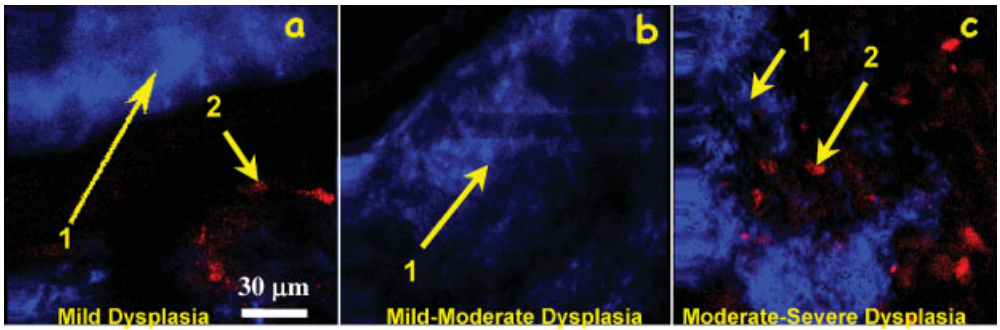


Fig. 4. MPM in vivo images of hamster cheek pouch dysplasia. The interstitial matrix (blue) (1) is only partially intact, with some areas of total collagen loss and other areas with variably reduced matrix structure and density. Collagen fibrils appear less linear, shorter, less structured (1) than in healthy tissue. Cellular exudate (2) is visible in (**a**) and (**c**). Imaging time points: (a) mild dysplasia—3 weeks DMBA, (**b**) mild-moderate dysplasia—4 weeks DMBA, (c) moderate-severe dysplasia—5 weeks DMBA.

Diagnostic sensitivity of MPM for differentiating between healthy (0–1) versus pathological (2–6) lesions was 98% (SE = 0.020) and specificity was 95% (SE = 0.049) if each score was considered separately (n = 140). Using this technique, each sample was counted twice, as each sample was evaluated separately by each of the two scorers. Using the consensus score (n = 70) from both investigators (in case of non-consensus, the average of the two scores was used), sensitivity for MPM was 100% and specificity was 90%.

Diagnostic sensitivity for differentiating between malignant (5–6) versus non-malignant (0–4) lesions was 95% (SE = 0.049) and specificity was 98% (SE = 0.020). Using the consensus score from both investigators (in case of non-consensus, the higher of the two scores was used), sensitivity for MPM was 100% and specificity was 96%.

Diagnostic sensitivity for differentiating between malignant (5–6) versus non-malignant (0–4) lesions was 98% (SE = 0.020) and specificity was 95% (SE = 0.049). Using the consensus score from both investigators (in case of non-consensus, the higher of the two scores was used), sensitivity for MPM was 100% and specificity was 96%.

## DISCUSSION

Oral carcinogenesis is a multi-step process in which genetic events lead to the disruption of the normal regulatory pathways that control basic cellular functions including cell division, differentiation, and cell death. Histopathologic progression from preneoplasia to cancer is accompanied by the accumulation of genetic alterations, which lead to modifications in protein structure and function. Tumor growth and metastasis depends upon angiogenesis, neovascularization, and extracellular matrix degradation. Morphological changes include hyperproliferation and nuclear crowding of basal cells. The epithelium frequently demonstrates thickening, loss of cell stratification, enlargement of epithelial cell nuclei, increased nuclear-to-cytoplasmic ratio, hyperchromasia, and pleopmorphism. Increased metabolic rate, inflammatory changes, and neovascularization are observed. The underlying connective tissue undergoes reorganization and degradation of parts of the basement membrane and underlying collagen network, facilitating tumour cell invasion and ultimately metastatic dissemination via the lymphatic and

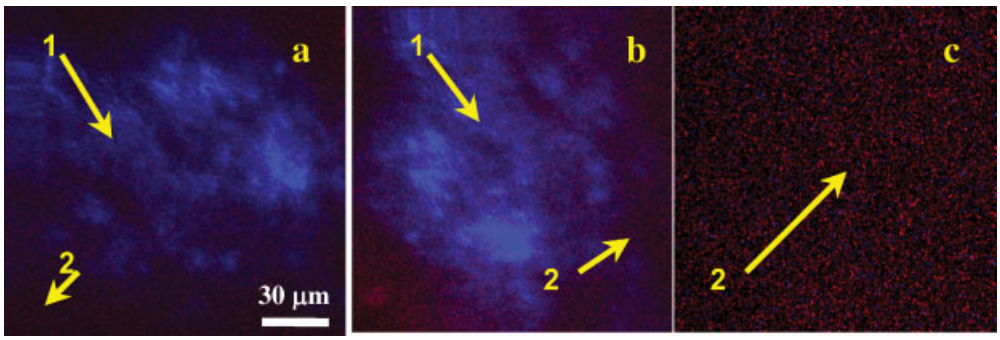


Fig. 5. Carcinoma-in situ (**a**), squamous cell carcinoma (s.c.c.) (**b**, **c**) imaged in vivo. Progressive loss over time of collagen structure and presence (1) (blue fluorescence) is seen. The normal collagen framework is replaced entirely by tumor cells (2) (red) in (c). Imaging time points: (a ) 8 weeks DMBA (carcinoma-in-situ) (b) 11 weeks DMBA (s.c.c.) (c) 15 weeks DMBA. (advanced s.c.c.).

**TABLE 2. Typical Diagnostic Scores From 35 Areas, Showing Grading of Pathology on a Scale of 0 (Healthy)–6 (Squamous Cell Carcinoma) Using H&E Stained Samples and MPM Images**

| | S1/1 | S1/2 | S2/1 | S2/2 | S3/1 | S3/2 | S4/.1 | S4/2 | S5/1 | S5/2 |
|---|---|---|---|---|---|---|---|---|---|---|
| Histo | 0 | 0 | 0 | 0 | 0 | 0 | 0 | 0 | 0 | 0 |
| MPM | 0 | 0 | 0 | 0 | 0 | 0 | 0 | 1 | 0 | 0 |
| | S6/1 | S6/2 | S7/1 | S7/2 | S8/1 | S8/2 | S9/1 | S9/2 | S10/1 | S10/2 |
| Histo | 1 | 1 | 1 | 1 | 1 | 1 | 1 | 1 | 1 | 1 |
| MPM | 1 | 1 | 1 | 1 | 0 | 1 | 1 | 1 | 2 | 1 |
| | S11/1 | S11/2 | S12/1 | S12/2 | S13/1 | S13/2 | S14/1 | S14/2 | S15/1 | S15/2 |
| Histo | 2 | 2 | 2 | 2 | 2 | 2 | 2 | 2 | 2 | 2 |
| MPM | 2 | 2 | 2 | 2 | 2 | 2 | 1 | 2 | 2 | 2 |
| | S16/1 | S16/2 | S17/1 | S17/2 | S18/1 | S18/2 | S19/1 | S19/2 | S20/1 | S20/2 |
| Histo | 3 | 3 | 3 | 3 | 3 | 3 | 3 | 3 | 3 | 3 |
| MPM | 3 | 3 | 3 | 3 | 3 | 3 | 4 | 4 | 3 | 3 |
| | S21/1 | S21/2 | S22/1 | S22/2 | S23/1 | S23/2 | S24/1 | S24/2 | S25/1 | S25/2 |
| Histo | 4 | 4 | 4 | 4 | 4 | 4 | 4 | 4 | 4 | 4 |
| MPM | 4 | 5 | 4 | 4 | 4 | 4 | 4 | 4 | 4 | 4 |
| | S26/1 | S26/2 | S27/1 | S27/2 | S28/1 | S28/2 | S29/1 | S29/2 | S30/1 | S30/2 |
| Histo | 5 | 5 | 5 | 5 | 5 | 5 | 5 | 5 | 5 | 5 |
| MPM | 4 | 5 | 5 | 5 | 5 | 5 | 5 | 5 | 5 | 5 |
| | S31/1 | S31/2 | S32/1 | S32/2 | S33/1 | S33/2 | S34/1 | S34/2 | S35/1 | S35/2 |
| Histo | 6 | 6 | 6 | 6 | 6 | 6 | 6 | 6 | 6 | 6 |
| MPM | 6 | 6 | 6 | 6 | 6 | 6 | 6 | 6 | 6 | 6 |

Diagnoses were performed by two pre-standardized, blinded investigators. MPM images were kept totally separate from and not matched in any way to histopathological images.
S1/1 denotes sample 1 diagnosed by scorer 1. S1/2 denotes sample 1 diagnosed by scorer 2.

vascular systems. However, a sequence- and spatially-resolved map of this multi-level process, permitting early diagnosis, prediction of lesion development and targeting of specific processes to achieve effective intervention is still not defined.

Using in vivo MPM, progressive carcinogenesis-related reduction in collagen fiber length, followed by breakdown and eventual loss of the regular collagen framework within the oral tissues were observed. While changes in the collagen fiber length and appearance were already visible during tissue inflammation, breakdown and loss of the collagen matrix became noticeable only after the onset of histologically evident dysplasia. Destruction of the extracellular matrix was extensive in s.c.c., with very little matrix remaining in advanced s.c.c. These results are in agreement with histological and immunohistochemical studies linking the carcinogenesis process with progressive decreases in extracellular matrix organization and presence [6–9].

**TABLE 3. Intra-Observer Variability Assessed Using 2 Scoring Sessions Separated by a 3 Month Interval**

| | Histopathology | | MPM/SHG | |
|---|---|---|---|---|
| | kappa | Se | kappa | se |
| Observer 1 | 0.933 | 0.046 | 0.920 | 0.054 |
| Observer 2 | 0.967 | 0.033 | 0.921 | 0.053 |
| Combined | 0.950 | 0.028 | 0.921 | 0.038 |

Capillaries, inflammatory infiltrates, and microtumors were clearly visible. The engorged appearance of blood vessels in inflamed tissues is in agreement with the hyperemia that is a feature of the inflammatory process. In dysplastic and malignant tissues, blood vessels only infrequently appeared obviously engorged. Perhaps the presence of a moderate degree of engorgement simply was not evident to the observers when compared to the obvious, extreme engorgement seen during inflammation only, earlier in the carcinogenesis process. The lateness of the main vascular or angiogenic phase in oral carcinogenesis—when a solid tumor mass is well established—may also be relevant [6]. The studies described in this paper focused primarily on the 10–15 week process of carcinogenesis, so

**TABLE 4. MPM Score Versus Histopathology Score—Combined Data From Both Scorers**

| | 0 | 1 | 2 | 3 | 4 | 5 | 6 | Total |
|---|---|---|---|---|---|---|---|---|
| 0 | 9 | 1 | 0 | 0 | 0 | 0 | 0 | 10 |
| 1 | 1 | 8 | 1 | 0 | 0 | 0 | 0 | 10 |
| 2 | 0 | 1 | 9 | 0 | 0 | 0 | 0 | 10 |
| 3 | 0 | 0 | 0 | 8 | 0 | 0 | 0 | 8 |
| 4 | 0 | 0 | 0 | 2 | 9 | 1 | 0 | 12 |
| 5 | 0 | 0 | 0 | 0 | 1 | 9 | 0 | 10 |
| 6 | 0 | 0 | 0 | 0 | 0 | 0 | 10 | 10 |
| Total | 10 | 10 | 10 | 10 | 10 | 10 | 10 | 70 |

Frequencies: MPM (rows) by histology (columns).

**TABLE 5. Agreement Between MPM Score and Histopathology Score**

| | Histopathology versus MPM | |
|---|---|---|
| | Kappa | Se |
| Observer 1 | 0.833 | 0.069 |
| Observer 2 | 0.900 | 0.055 |
| Combined | 0.867 | 0.044 |

that this main vascular phase may well not have developed by the time the animals were sacrificed.

Microtumors were consistently observed in malignant tissues. Further studies using this modality should provide a better understanding of the timing, localization, and spread of these microtumors, providing researchers with a better understanding of the process of tumor proliferation and spread.

Intra- and inter-observer variability with regard to diagnosis was acceptable, with discrepancies between the evaluators never exceeding one point. Sensitivity was very good in general and excellent for s.c.c. There is potential for discriminatory improvement as the capabilities of this modality develop further.

These preliminary studies confirm the usefulness of high-resolution, in vivo imaging as a promising tool for clinical and research needs related to oral premalignancy and malignancy. Further studies are underway to engineer higher resolution systems with improved flexible fiberoptic probe capabilities. These will facilitate the development of new approaches to the clinical diagnosis and management of oral pathologies, and to a better understanding of the processes predicting and paralleling premalignant and malignant change. In the future, these capabilities will permit investigation in patients into the effects of chemoprevention and chemotherapy on the parameters described above, providing a better understanding of pathological mechanisms, predictors of malignant change in dysplasia, risk of tumor recurrence, and predictors of tumor response to therapy.

## REFERENCES


1. Cancer facts and figures. American Cancer Society Report 2000; p 4.
2. Regezi J, Sciubba J, editors. Oral pathology. Philadelphia: W.B.Saunders Co; 1993. pp 77–90.
3. California department of health services. Cancer Surveillance Section Annual Report 1999.
4. Slaughter DP. Field cancerization in oral stratified squamous epithelium. Cancer 1953;6:963–968.
5. Georgakoudi I, Jacobson BC, Muller MG, Sheets EE, Badizadegan K, Carr-Locke DL, et al. NAD(P)H and collagen as in vivo quantitative fluorescent biomarkers of epithelial precancerous changes. Cancer Res 2002;62(3):682–687.
6. Mohamed KM, Le A, Duong H, Wu Y, Zhang Q, Messadi DV. Correlation between VEGF and HIF-1a expression in human oral squamous cell carcinoma. Exp Mol Pathol 2004;76:143–152.
7. Aznavoorian S, Moore BA, Alexander-Lister LD, Hallit SL, Windsor LJ, Engler JA. Membrane type I-matrix metalloproteinase-mediated degradation of type I collagen by oral squamous cell carcinoma cells. Cancer Res 2001;61(16): 6264–6275.
8. Ziober BL, Turner MA, Palefsky JM, Banda MJ, Kramer RH. Type I collagen degradation by invasive oral squamous cell carcinoma. Oral Oncol 2000;36(4):365–372.
9. Jiang DJ, Wilson DF, Smith PS, Pierce AM, Wiebkin OW. Distribution of basal lamina type IV collagen and laminin in normal rat tongue mucosa and experimental oral carcinoma: Ultrastructural immunolocalization and immunogold quantitation. Eur J Cancer B Oral Oncol 1994;4: 237–243.
10. Konig K. Multiphoton microscopy in life sciences. J Microsc 2000;200:83–104.
11. Williams RZWR, Webb WW. Multiphoton microscopy in biological research. Curr Opin Chem Biol 2001;5:603–608.
12. Hecht E. Optics, 3rd edn. New York: Addison Wesley Longman, Inc.; 1998.
13. Saleh BE. Fundamentals of photonics. New York: Wiley; 1991.
14. Shen YR. Principles of nonlinear optics. New York: Wiley; 1984.
15. Campagnola PJWM, Lewis A, Loew LM. High-resolution nonlinear optical imaging of live cells by second harmonic generation. Biophys J 1999;77:3341–3349.
16. Gauderon R, Lukins PB, Sheppard CJ. Optimization of second-harmonic generation microscopy. Micron 2001;32: 691–700.
17. Gauderon R, Lukins PB, Sheppard CJ. Simultaneous multichannel nonlinear imaging: Combined two-photon excited fluorescence and second-harmonic generation microscopy. Micron 2001;32:685–689.
18. Fine S, Hansen WP. Optical second harmonic generation in biological systems. Appl Opt 1971;10:2350–2353.
19. Georgiou E. Second and third optical harmonic generation in type I collagen, by nanosecond laser irradiation, over a broad spectral region. Opt Commun 2000;176:253–260.
20. Kim B, Eichler J, Reiser K, Rubenchik AM, Da Silva LB. Collagen structure and nonlinear susceptibility: Effects of heat, glycation, and enzymatic cleavage on second harmonic signal intensity. Lasers Surg Med 2000;27:329–335.
21. Guo Y. Subsurface tumor progression investigated by noninvasive optical second harmonic tomography. Proc Natl Acad Sci USA 1999;96:10854–10856.
22. Masters BR, So P, Gratton E. Multiphoton excitation microscopy of in vivo human skin. Ann NY Acad Sci 1998; 838:58–67.
23. Masters BR, So P. Multiphoton excitation microscopy. Opt Express 2001;8:2–10.
24. Agarwal A, Coleno ML, Wallace WP, Wu WY, Sun CH, Tromberg BJ, George SC. Two-photon laser scanning microscopy of epithelial cell-modulated collagen density in engineered human lung tissue. Tissue Eng 2001;7:191–202.
25. Diaspro A, Robello M. Two-photon excitation of fluorescence for three-dimensional optical imaging of biological structures. Photochem Photobiol 2000;55:1–8.
26. Zoumi A, Yeh A, Tromberg BJ. Imaging cells and extracellular matrix in vivo using SHG and TPEF. PNAS 2002; 99(17):11014–11019.
27. Campagnola J, Millard A, Terasaki M, Hoppe PE, Malone CJ, Mohler WA. Three-dimensional high-resolution second-harmonic generation imaging of endogenous structural proteins in biological tissues. Biophys J 2002;81:493–508.
28. Brown EMT, diTomaso E, Pluen A, Seed B, Boucher Y, Jain RK. Dynamic imaging of collagen and its modulation using SHG. Nat Med 2003;9(6):796–801.
29. MacDonald DG. Comparison of epithelial dysplasia in hamster cheek pouch carcinogenesis and human oral mucosa. J Oral Pathol 1981;10:186–191.
30. Wilder-Smith P, Liaw L, Krasieva TB, Messadi D. Laser-induced fluorescence for detection and diagnosis of oral malignancy. J Dent Res 1999;78:820.
31. Wilder-Smith P, Liaw L, Krasieva TB, Nguy L, Yoon Y, Messadi D. Topical ALA-induced fluorescence in oral dysplasia and malignancy. Lasers Surg Med 1999;69:39.